Light Metals 2013 *Edited by: Barry Sadler*
TMS (The Minerals, Metals & Materials Society), 2013

Thermo-electro-mechanical characterization of anode interfaces at operating conditions

Hugues Fortin[1], Marie-Hélène Martin[2, 3], Nédeltcho Kandev[1], Guillaume Gauvin[2], Donald Ziegler[3] and Mario Fafard[2]

[1]Institut de Recherche d'Hydro-Québec (IREQ), 600 avenue de la Montagne, Shawinigan (Québec), Canada, G9N 7N5
[2]NSERC/Alcoa Industrial Research Chair MACE[3] and Aluminium Research Centre-REGAL, Université Laval, Quebec City (Québec), Canada, G1V 0A6
[3]Alcoa Canada, 1 blvd. des Sources, Deschambault-Grondines, QC, G0A 1S0, Canada

Keywords: Aluminium reduction cell, anode connection, anode stub contact, anode power losses, electrical contact resistance, thermal contact conductance

Abstract

A large amount of energy is lost at the interface between materials in electrodes, reducing process energy efficiency. Thus, the characterization of thermo-electro-mechanical behaviour of the interfaces is necessary to support the numerical modelling as an essential step in improving the design of the anode connection. Experiments have been performed on carbon-cast iron-steel samples taken from the anode assembly. The samples have been designed and prepared in such a way that they are representative of the industrial sealing process.

Some links between roughness and electrical resistivity have already been established in other studies [1]. In the present investigation, roughness measurements using laser profilometry have been carried out on samples subjected to compressive stress up to 2 MPa. Results have shown that loading effect is negligible on the asperities deterioration between the carbon-cast iron interfaces at this pressure.

The obtained values of thermal contact resistance (TCR) and electrical contact resistance (ECR) are in good agreement with the experimental data published in the literature, but still higher than those of the theoretical contact model. This study leads to the development of a new constitutive law for electrical and thermal contact resistance as a function of temperature and pressure.

Introduction

In 2003, the U.S. aluminum roadmap aimed for energy consumption of 11 kWh/kg of Al to the year 2020. To achieve this goal, many investigations have been conducted on the development of complex numerical models used to test new energy efficient designs of the Hall-Héroult cell. As shown by the measurements of Wilkening and Côté [2], about 120 mV are lost in the carbon-cast iron-steel interfaces. Typical voltage drop in a prebake anode is 300 mV, as pointed out by Choate and Green [3]. Therefore, one of the promising areas is the development of new anode connection designs that can significantly decrease the power losses at the interfaces.

The anode connection assembly consists of steel stubs inserted into predefined holes in a carbon block made of coke and pitch. To hold the steel stub and the carbon anode together, liquid cast iron is poured between them, sealing the assembly. When the cast iron cools down, an air gap between the carbon and the cast iron is created. In operation, as temperature increases in the stub hole, the steel stub and cast iron thimble dilate, creating mechanical pressure on the carbon and closing the air gap. This phenomenon facilitates the transmission of the thermal and electrical flux through the interfaces. Thus, the carbon-cast iron-steel interfaces involve complex interactions between non-linear thermal, electrical, mechanical and surface phenomena. A better understanding of the thermo-electro-mechanical (TEM) behavior of the anode connection interfaces is needed to predict the thermal contact resistance (TCR) and the electrical contact resistance (ECR) as a function of both pressure and temperature.

To characterize the TCR and the ECR, a lab-scale reproduction of the operating condition in the anode assembly has been developed [4]. Carbon-cast iron-steel samples have been created using a new technique to represent the industrial sealing process. Using the apparatus developed by Kandev et al. [5], new constitutive laws for the carbon-cast iron and cast iron-steel interfaces in the anode assembly have been determined. These new laws will be incorporated into a finite element (FEM) code and will support the development of new anode connection designs, as pointed out recently in the literature by several authors [6-10].

Previous work

In the nineteen seventies, Peterson [11] measured the voltage drop in several spots in the anode and found that the carbon-cast iron-steel interface was responsible for up to 25% of the overall voltage drop in the anode. Two years later, Peterson [12] concluded that electrical contact resistance at high temperature was negligible, which seemed at this point to contradict results published two years before. In 1984, Brooks and Bullough [13], while attempting to optimize cast iron thimble thickness without cracking the anode, found that ECR was a function of both temperature and contact pressure. These works have paved the way to the development of lab-test apparatus to characterize the ECR.

In the nineteen nineties, Sørlie and Gran [14] built an apparatus to measure the ECR of cathode carbon-steel interfaces as a function of both temperature and pressure to help increase the energy efficiency in the cell. The apparatus was later reused by Hiltmann et al. [15] to characterize the carbon-cast iron interfaces. From these experiments, unfortunately, no constitutive laws were developed for ECR.

Reproducing the Sørlie and Gran [14] experiment at room temperature for anode carbon material, Richard et al. [16, 17]

were able to develop a constitutive law for ECR as a function of both temperature and pressure in the form of a Weibull function. With this law, they were able to incorporate it in a FEM TEM model to optimize the stub hole configuration.

In 2003, Laberge et al. [18] built a new test bench to characterize the anode-coke bed-cathode interfaces during the preheating of the cell based on the same principle as the Sørlie and Gran [14] experiment. Adapting the test bench for the carbon-cast iron-steel interfaces of both anode and cathode, Rouleau [19] and St-George et al. [20] found that the experimental TCR and ERC constitutive values were higher than those of the theoretical model.

Sample preparation

Based on previous research [14, 15, 19], samples should be made in such a way that they represent the surface characteristics of actual anode connections. To obtain a more accurate representation of the contact interfaces, 2-inch cylindrical samples were made with a carbon-cast iron-steel sandwich instead of treating the carbon-cast iron and cast iron-steel interfaces separately.

For the steel part, the cylindrical samples were machined. However, for the carbon, it was difficult to obtain flat and parallel surfaces by taking samples in the region of the stub hole. To overcome this problem, samples were taken from the side surface in the bottom of the anode, perpendicular to the anode slot (See Figure 1). The following hypothesis was made: the horizontal and vertical forces in the slot area, acting on the green anode during the vibro-compaction are the same as those in the stub hole area.

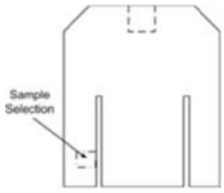

Figure 1: Area of the core samples in the anode

A mold was designed in such a way that liquid cast iron used for the sealing process was poured into an opening between the steel and the anode carbon. The mold was manufactured from a cathode carbon block where a two-inch diameter hole was machined through the block where carbon and steel were placed at each end of the block. Figure 2 represents the middle part of the mold with the detail of each part. The channel on the top of the mold was drilled to facilitate the hot gas evacuation. Before pouring the cast iron, the mold was preheated at 100°C to remove the moisture.

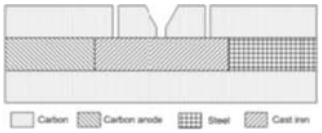

Figure 2: Middle part of the mold used to make the sample

Once the sample was cooled at the same rate as in the industrial process, the assembly was carefully removed from the mold to ensure that the asperities of the carbon and cast iron surface were not altered. Figure 3a shows the final result of the carbon-cast iron-steel sandwich. The position of the thermocouple in the samples is displayed in Figure 3b. Due to the non-linear behavior of the carbon, four thermocouples were used and only three used in the cast iron. For the steel, five thermocouples were used to increase the precision of the thermal flux calculation.

To evaluate the effect of the casting procedure, two random samples were separated into three parts in addition to the three samples used for the ECR and TRC characterization once the data were collected on the test bench. Visual inspection showed that the asperities at the carbon-cast iron interfaces were very large as compared with the smooth surface of the cast iron-steel interface. However, surface inspection of these five different samples revealed no trace of weld spot at the cast iron-steel interfaces.

Figure 3a): Sample assembly

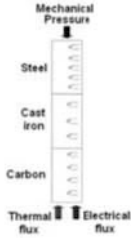

Figure 3b): Thermocouple position and sample parts

The sample instrumentation was constructed using type K special limits thermocouples and the data were measured with an Agilent 34970A acquisition system set at a five-second time step. To measure the voltage drop and the temperature gradient in the anode, one-eighth-inch-diameter holes were drilled carefully in each part of the sample. Temperature was measured directly with the thermocouple, while the voltage drop was measured between two different thermocouples on the acquisition card. Pyro-duct 597A silver paste was used to bond the thermocouple in the steel and cast iron hole. For the thermocouple located in the carbon, the holes were filled with graphite powder.

Preliminary tests were performed on the sample to determine the effect of depth of thermocouple penetration on the temperature distribution. Two different configurations (half-inch and quarter-inch depth) are compared in Figure 4 and results show that there was no difference between the two depths.

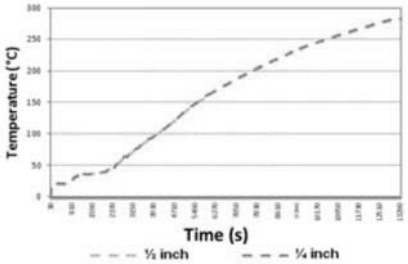

Figure 4: Measured temperature in function of time for two different depths

With the instrumentation of the sample completed, the ECR, based on Sørlie and Gran's work [14], can be calculated from Equation 1. By extrapolating the voltage drop measured at the interfaces and knowing the electrical current that passes through the entire sample, ECR can be calculated:

$$ECR\ (T,P) = \frac{\Delta U_{21}}{I} \quad (1)$$

The determination of the thermal flux at the interface is tricky. Fourier's law (Equation 3) represents the unidirectional thermal flux by conduction. By characterizing the thermal conductivity (k) as a function of the steel temperature (Figure 5), thermal flux can be extrapolated at the interface.

$$q'' = -k(T) \cdot \frac{dT}{dz} \quad (2)$$

Using the same approach as Singhal et al. [21] described in Equation 3, the TCR can be calculated.

$$TCR\ (T,P) = \frac{\Delta T_{21}}{q} \quad (3)$$

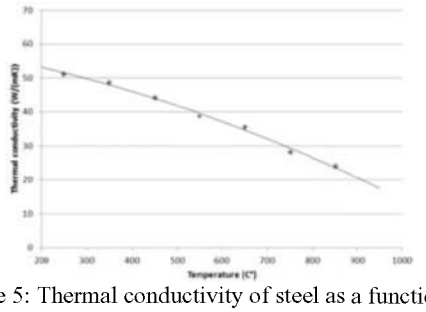

Figure 5: Thermal conductivity of steel as a function of temperature

Experimental apparatus

The experimental apparatus [5], shown in Figure 6, was used to reproduce the TEM behavior of the stub hole in operating conditions. Knowing that thermal gradient is upwards in the anode assembly, the same configuration was used, such that the heat transfer started from the carbon, to the cast iron and to the steel.

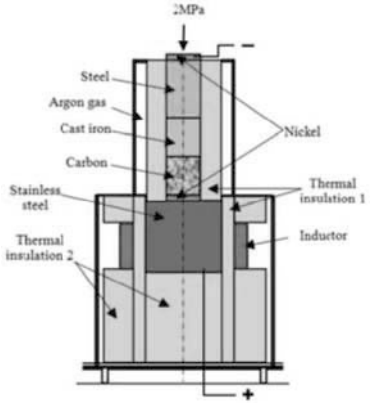

Figure 6: Apparatus sketch

For the thermal heat generation, induction heating was selected rather than the use of a furnace. The main advantage of this technology is that temperature equilibrium can be reached very quickly while precisely controlling the power injected into the sample. Several thermocouples were used to measure the temperature and the voltage in the different parts of the sample, as well as on the billet and the nickel disk to ensure that the thermal limits of the materials were respected.

The apparatus was built using cylindrical copper coil wrapped around a stainless steel billet to create induction coils. Using a 30 kW power generator operating at 3 kHz, the magnetic field generates Foucault currents, which, by Joule's effect, increase the temperature of the stainless steel billet. The billet acts as a heat generator modulated by the input power, where the heat is transferred to the sample by conduction. To prevent overheating of the copper coil at high induction heating power, the coil is water-cooled.

In order to minimize heat losses, a high-quality thermal insulation (thermal insulation 1) was wrapped around the sample and around the stainless steel billet. This configuration also limited the outgoing radial heat flux and ensured that the thermal gradient was vertical in the sample. Several layers of a special thermal insulation (thermal insulation 2), resistant to high mechanical pressure and high temperature, were placed under the billet for thermal insulation and mechanical support purposes. To ensure that the electrical flux lines were perpendicular to the interfaces, two nickel disks were placed at both ends of the carbon-cast-iron-steel sample.

To limit the effect of air oxidation at high temperature, the billet was placed in a cylindrical casing made of nylon and G9 composite material. On the top of the casing, a stainless steel cylindrical shell was bolted in to protect the sample and seal the volume. Argon gas was inserted in both parts of this assembly with a positive pressure to create a controlled inert gas environment. The argon gas flow was carefully monitored to minimize the local decreases of temperature while minimizing the oxidation effect.

A DC electrical field was applied between the stainless steel billet and the upper nickel disk to drive a uniform DC current through the samples. For the mechanical pressure, the sample placed between the nickel disks was mounted on a mechanical press designed for this purpose. A pancake load cell (Intertechnology SW10-2KB000) was used to measure the force acting on the sample. The final design of the apparatus in operating condition can be seen in Figure 7.

Figure 7: Testing apparatus

Profilometry study

It is well known that the surface topography greatly influences the TCR and the ECR. As pointed out by Singhal et al. [21], asperities tend to deform at the surface when applying loading-unloading cycle, decreasing the TCR until it reaches an

equilibrium state. The damage of the asperities decreases the contact area, and in the same way increases the TCR.

For this reason, the effect of pressure variation on the carbon-cast iron interfaces was investigated in this study. Picard et al. [22] concluded that, on semi-graphitic carbon cathode material, the effect of pressure below 10 MPa did not induce any damage in the sample. Assuming that carbon anode behaviour is similar to that of a semi-graphitic carbon cathode, a pressure of 2 MPa should not significantly modify the surface asperities of carbon.

In order to validate this hypothesis, the steel portion from two samples was removed and only the carbon and cast iron contact surfaces were characterized by laser profilometry. A surface sample was scanned along parallel lines with a distance of 40 µm between subsequent lines. Output results are given in a form of a 1080*1200 pixel 2D matrices (X, Y). An example of asperity characterization of carbon surface can be seen in Figure 8 using a MATLAB imaging script.

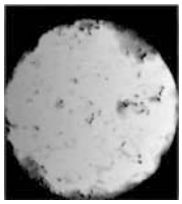

Figure 8: Carbon surface laser profilometry

Respecting the ASME B46.1 [23], the RMS surface roughness as well as the mean slope for both carbon and cast iron samples were measured six times to estimate the experimental errors. While holding the initial alignment intact, a mechanical press applied a pressure of 2 MPa on the sample at room temperature. Once done, laser profilometry was carried out two more times on the carbon and on the cast iron surface to characterize the loading effect. Preliminary analysis shows that some asperities in the cast iron are in the order of 2-3 mm in height.

Figure 9 presents the surface roughness RMS for the two different samples. Results show that the mean value of the surface roughness after the loading is slightly modified from the initial value, but it cannot be differentiated from the experimental errors. From these experiments, it is possible to conclude that mechanical pressure of 2MPa did not significantly modify the surface asperities and bias the TCR and ECR.

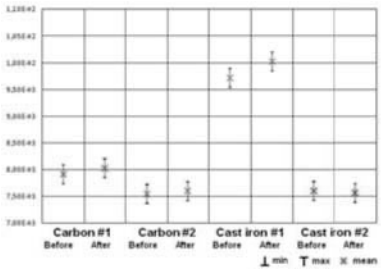

Figure 9: Roughness RMS before and after load application

Experimental protocol

The experimental characterization of the TCR and the ECR was carried out on three different samples. From the results published in the literature [13, 20], at a pressure higher than 2 MPa, a plateau is reached and increasing the pressure does not seem to have an effect on the ECR and TCR. Thus, measurements were made at pressures of 175 kPa, 375 kPa, 0.5 MPa, 1 MPa, 1.5 MPa and 2 MPa. Due to the temperature gradient in the samples, measurements were taken when the temperature in the lower thermocouple in the carbon reached 300 °C, 400 °C, 700 °C and 975 °C.

For the electrical field, preliminary tests showed that voltage drop was difficult to measure using a current density of 1A/cm^2 due to the low electrical resistivity of the steel. For this reason, tests were performed using a current of 150 A in order to measure the voltage drop in the steel.

Having validated previously that an axial stress of 2 MPa does not significantly modify the surface properties, a sample can be heated at different temperatures and subjected to different pressures without appreciably damaging the surface properties. Thus, for the first temperature step, a mechanical pressure of 2 MPa was applied to the sample to reduce the heating time. Once the thermal equilibrium was reached, in about one to two hours, measurements were taken. Next, a mechanical pressure of 1.5 MPa was applied to the sample until temperature equilibrium and so on to scan the entire pressure range. Once done, temperature was increased to the next target point and the unloading cycle was started. Typically it takes six to eight hours to scan the entire pressure range for a given temperature. In this manner, tests were performed over a four-to-five day span, each day corresponding to a target temperature.

Finally, to validate the experimental set-up pertaining to the carbon oxidation, a comparison of the initial and final carbon weight was made. Results showed that the oxidation was less than 2% (195g before and 193g after) of initial weight, confirming that the experimental set-up minimized the oxidation effect.

Results

Different thermocouples located within the sample measured the temperature and the voltage drop in each of the materials. Figure 10 presents the temperature as a function of position in the sample at a pressure of 175 kPa. The diminution of temperature at the interfaces is quite significant at such a low pressure. Based on these results, temperature can be extrapolated at the interfaces, and afterward, the thermal flux that leads to the TCR calculation can be estimated.

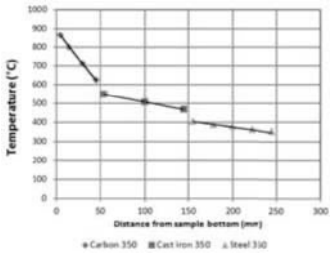

Figure 10: Temperature in the sample as a function of position at a pressure of 175 kPa

Figures 11 and 12 show the TCR as a function of pressure at different temperatures for the carbon-cast iron and cast iron-steel interfaces. As expected, results show that the TCR decreases as

temperature and pressure increase. Also, for a given temperature, the TCR tends to reach a plateau over a pressure of 2 MPa. The same phenomena are observed for both interfaces.

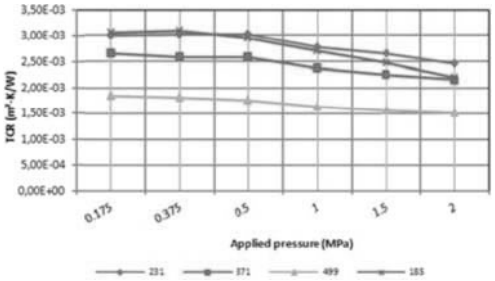

Figure 11: Thermal contact resistance as a function of both temperature and pressure for Carbon-Cast iron interfaces

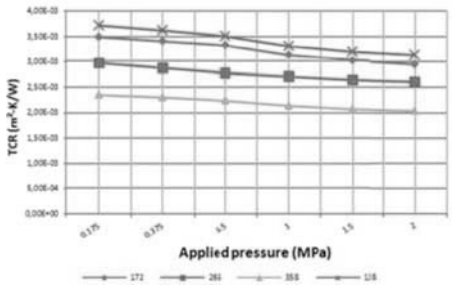

Figure 12: Thermal contact resistance as a function of both temperature and pressure for Cast iron-Steel interfaces

Using the same technique, the ECR was calculated from the voltage drop measurements in the sample. Figures 13 and 14 show the ECR as a function of both temperature and pressure for the two different interfaces.

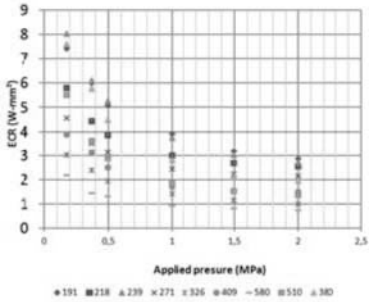

Figure 13: Electrical contact resistance as a function of both temperature and pressure for Carbon-Cast iron interfaces

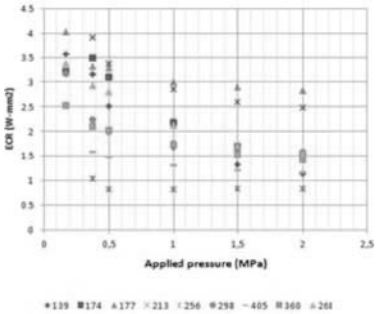

Figure 14: Electrical contact resistance as a function of both temperature and pressure for Cast iron-Steel interfaces

Results show that a plateau is reached for an axial load over 2 MPa, confirming the range chosen earlier. Also, results show that pressure has more effect on ECR than TCR. It can be seen on Figure 13 that for the ECR, high temperature influences the quickness reaching of the plateau. This is mainly due to the effect of thermal dilatation of the asperities that increases the real contact area and by same way, increases the conduction of the interface.

Using MATLAB® statistical toolbox, several laws were tested to create a fit for these values. Best results were obtained using power function for both TCR and ECR as shown by Equation (4). In this case, the fitting constant A and B could be linear or quadratic function of temperature, depending on the case.

$$\boldsymbol{Contact\ Resistance}(T,P) = A \cdot P^{B} \qquad (4)$$

To validate the experimental results, an ANOVA was run to verify if the increase in model complexity diminished the sums of square error (SSE) of the fitting model by using the Fisher-Snedecor test. Results show that in some cases, thermal dependency of the fitting constant does not significantly decrease the SSE of the model. As a resultant, the ECR of the cast iron-Steel interface is only a function of the applied pressure, as the two coefficients are not temperature dependent.

Constitutive laws were plotted and compared with the results presented by Rouleau [19]. Experimental results for the TCR and ECR are higher for each interface at low temperature. However, as temperature increases, the results tend toward the same value. As presented in Figure 15, similar behavior is shown in temperature and pressure variation and the order of magnitude is confirmed.

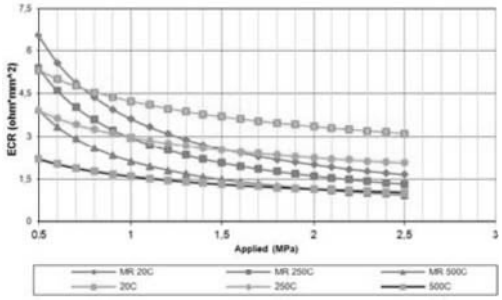

Figure 15: Comparison of experimental results (Solid curves) and Rouleau [17] (Dot curves) for the electrical contact resistance of Carbon-Cast iron interface

This divergence from the data published by Rouleau [19] can be explained by the use of different surface properties that resemble those of the industrial interface in the stub hole.

Conclusion

Using the apparatus developed by Kandev et al. [5], the characterization of the thermal contact resistance and the electrical contact resistance have been completed for the carbon-cast iron-steel interfaces in the anode connection. Results have shown that the values for the TCR and ECR are in conformity with the experimental data published in the literature, but are still higher than those provided by the theoretical contact model. This difference could be due to the

surface properties of the samples that have been based on the reproduction of the industrial interfaces in the cell.

The samples were made using a new molding technique different from the one published in the literature. In this configuration, carbon-cast iron and the cast iron-steel interfaces were characterized in a single step. Carbon oxidation measurements showed that the weight reduction was less than 2%, having negligible impact on the TCR and ECR characterization.

Laser profilometry was carried out on samples to measure the effect of loading on the asperities degradation up to a pressure of 2 MPa. Results indicated that charge effect was negligible on the asperities deterioration between the carbon-cast iron interfaces at this pressure.

Constitutive laws have been obtained for the TCR and the ECR as a function of both temperature and pressure. These laws will be incorporated into a FEM code to study the anode connection behavior, especially the stub hole design, to achieve energy savings in the future.

Acknowledgements

The authors would like to thank Simon Gélinas from Laval University, Sylvain Chénard and François St-Onge from IREQ for the experimental test measurements. We also want to thankDonald Picard from Laval University for the useful discussion about the mechanical behavior of the carbon anode and Michel Gasse from Alcoa-Deschambault for the sample preparation, especially the cast iron casting manipulation. A portion of the research presented in this paper was financed by the *Fonds québécois de la recherche sur la nature et les technologies* by the intermediary of the Aluminium Research Centre – REGAL, Natural Sciences and Engineering Research Council of Canada and Alcoa.

References

1. R. Holm: Electric Contact Theory and Applications, Springer-Verlag, New York, 1967.
2. Wilkening and Côté: Problems of the stub-anode connection, In Proc. TMS Light Metals, pp. 865-873, 2007.
3. W.T. Choate and J.A.S. Green, 2003. U.S. energy requirements for aluminum production: historical perspective, theoretical limits and new opportunities, Dept.of Energy, USA.
4. M.-H. Martin, 2013. Caractérisation des interfaces acier-fonte-carbone de l'ensemble anodique d'une cuve d'électrolyse d'aluminium, Master thesis, Université Laval, Québec, Canada.
5. N. Kandev, H. Fortin, S. Chénard, G. Gauvin, M.-H. Martin and M. Fafard: New apparatus for characterizing electrical contact resistance and thermal contact conductance, In Proc. TMS Light Metals, pp. 1003-1008, 2011.
6. H.Fortin, M. Fafard, N. Kandev and P. Goulet: FEM analysis of voltage drop in the anode connector assembly. In Proc. TMS Light Metals, pp. 1055-1060, 2009.
7. D. Richard, P. Goulet, O. Trempe, M. Dupuis and M. Fafard: Challenges in stub hole optimization of cast iron rodded anodes. In Proc. TMS Light Metals, pp. 1067-1071, 2009.
8. M. Dupuis. Development and application of an ANYS based thermo-electro-mechanical anode stub hole design tool. In Proc. TMS Light Metals, pp. 433-438, 2010
9. S. Beier, J.J.J. Chen, H. Fortin and M. Fafard: FEM analysis of the anode connection in aluminium reduction cells, In Proc. TMS Light Metals, pp. 979-984, 2011
10. D. Molenaar, K. Ding and A. Kapoor: Development of industrial benchmark finite element analysis model to study energy efficient electrical connections for primary aluminium smelters, In Proc. TMS Light Metals, pp. 985-990, 2011.
11. R.W. Peterson: Temperature and voltage measurements in Hall cell anodes. In Proc. TMS Light Metals, pp. 365-382, 1976.
12. R.W. Peterson: Studies of stub to carbon voltage. In Proc. TMS Light Metals, pp. 367-378, 1978.
13. D. G. Brooks and V. L. Bullough: Factors in the design of reduction cell anodes. In Proc. TMS Light Metals, pp. 961-976, 1984.
14. M. Sørlie and H. Gran: Cathode collector bar to carbon contact resistance. In Proc. TMS Light Metals, pp. 779-787, 1992.
15. F. Hiltmann, J. Mittag, A. Støre and H. A. Øye: Influence of temperature and contact pressure between cast iron and cathode carbon on contact resistance. In Proc. TMS Light Metals, pp. 277-283, 1996.
16. D. Richard, M. Fafard, R. Lacroix, P. Cléry and Y. Maltais.: Aluminum reduction cell anode stub hole design using weakly coupled thermo-electro-mechanical finite element models. Finite elements in analysis and design 37, pp. 287-304, 2001.
17. D. Richard, M. Fafard, R. Lacroix, P. Cléry and Y. Maltais: Carbon to cast iron electrical contact resistance constitutive model for finite element analysis. Journal of Materials Processing technology 132, pp. 119-131, 2003.
18. C. Laberge, L. Kiss and M. Desilets: The influence of the thermo-electrical characteristics of the coke bed on the preheating of an aluminum reduction cell, In Proc. TMS Light Metals, pp. 207-211, 2004.
19. M. Rouleau, 2007. Caractérisation thermo-électro-mécanique des interfaces fonte-acier-carbone dans une cuve d'électrolyse, Master thesis, Université du Québec à Chicoutimi (UQAC), Québec, Canada.
20. L. St-Georges, L. I. Kiss and M. Rouleau: Evaluation of contact resistance in electrodes of Hall-Héroult process, In Proc. TMS Light Metals, pp. 1103-1108, 2009.
21. V. Singhal, P. J. Litke, A. F. Black and S. V. Garimella: An experimentally validated thermo-mechanical model for the prediction of thermal contact conductance, International Journal of Heat and Mass Transfer 48, pp. 5446-5459, 2005.
22. D. Picard, M. Fafard, G. Soucy, J.-F. Bilodeau: Room temperature long-term creep/relaxation behavior of carbon cathode material, Materials Science and Engineering A, 496, pp. 366-375, 2008.
23. ASME B46.1, 2002 "Surface texture, surface roughness, waviness and lay"